Nanoscale Advances

ROYAL SOCIETY OF CHEMISTRY

PAPER

View Article Online
View Journal | View Issue

Cite this: *Nanoscale Adv.*, 2022, **4**, 521

2-Dimensional layered molybdenum disulfide nanosheets and CTAB-assisted molybdenum disulfide nanoflower for high performance supercapacitor application

H. Ganesha,[a] S. Veeresh,[a] Y. S. Nagaraju,[a] M. Vandana,[a] M. Basappa,[a] H. Vijeth[b] and H. Devendrappa *[a]

In this study, the supercapacitor performance of the hydrothermal synthesized molybdenum disulfide (MoS_2) nanosheets and the cetyltrimethylammonium bromide (CTAB)-assisted MoS_2 nanoflower morphology have been investigated. The as-synthesized MoS_2 nanoflower and nanosheet morphology structures were investigated *via* field emission scanning electron microscopy (FESEM), and the internal microstructure was examined *via* high resolution-transmission electron microscopy (HR-TEM) technique. The Fourier transform infrared (FT-IR) spectra were obtained to identify the chemical interaction and the functional groups present in the material. The shifting of the binding energy, oxidation states, and elemental identification were conducted by X-ray photon spectroscopy (XPS). The MoS_2 nanoflower possesses surface defects, which produce numerous active sites. The MoS_2 nanoflower and nanosheet electrodes demonstrate the high specific capacitance (C_{sp}) values of 516 F g^{-1} and 438 F g^{-1}, respectively, at a current density of 1 A g^{-1}. However, the MoS_2 nanoflower shows high C_{sp} due to the large surface area with active edges, making them store more energy in the electrode.

Received 4th September 2021
Accepted 2nd November 2021

DOI: 10.1039/d1na00664a

rsc.li/nanoscale-advances

1. Introduction

In the modern world, energy plays a predominant role in various applications, like energy storage and conversion, electronics devices, optical portable devices, laptops, computers, mobiles, and routine human daily domestic needs. The electrochemical energy storage technology is one of the emerging fields that provides solid-state batteries, fuel cells, and supercapacitors.[1–5] Among these, supercapacitors have attracted more attention because of their higher power density than the batteries, quick charging time, slow discharging time, more storage capacity, and longer durability than a conventional capacitor. Unfortunately, the practical application of the supercapacitor device could not achieve full success in large industrial production due to drawbacks, like poor cyclic stability, limited operating voltage, and chemical leakage. Therefore, the researchers are more focused on developing a new electrode material with high C_{sp}, good cyclic retention, wide operating voltage, and chemical stability. The strategy has been made to overcome these issues by adopting the well-controlled synthesis of nanomaterials with large surface area nanosheets, nanoflowers, and optimized morphology. The most significant morphology of the material may enhance the large surface area, chemical stability, and electrical conductivity; these are helpful in electrochemical energy storage applications. Recently, the development of an energy storage system as an effective clean energy carrier system was achieved, and replaced the non-renewable fossil fuels. Therefore, researchers traced out a variety of 2-D nanomaterials for energy storage and conversion applications, like fuel cells, batteries, and supercapacitors. Presently, the supercapacitor is a highly demanded device in energy storage and conversion systems.[6–8] The supercapacitor is categorized into two types, the pseudocapacitor and electrical double layer capacitor.[9,10] The pseudocapacitor is a faradaic reversible redox reaction process. An electrical double layer capacitor is a collection of charge separation and an interface between the electrode and electrolytes.[11,12] Transition metal sulfides (TMSs), such as CuS/Cu_2S,[13,14] NiS,[15] $MoSe_2$[16] SnS_2,[17] ZnS,[18] CoS,[19] FeS,[20] MoS_2, and WS_2,[21,22] have been exhaustively studied as an electrochemically active material for supercapacitor performance. MoS_2 is a highly studied TMSs compared to other metal sulfides, as well as the most important material scientifically and for industrially applications because of the different oxidation state with polymorphism, distinctive surface morphology structure, atomic structure, tremendous physical, chemical stability, electroactive properties, direct band gap, and small thickness, unique layered structure, wide

[a]*Department of Physics, Mangalore University, Mangalagangothri, 574199, India. E-mail: dehu2010@gmail.com*

[b]*Department of Physics, Mangalore Institution of Technology and Engineering, Badaga Mijar, Moodbidri, 574225, Karnataka, India*

specific surface area, good specific capacitance, and reported high electrochemical properties.[23,24] This material is assembled by weak van der Waals force and connected with a covalent bond sandwich between the S–Mo–S tri-layers closely linked with Mo and S atoms. This layered material can be categorized into three types: 1T MoS_2 trigonal, 2H MoS_2 hexagonal, and 3R MoS_2 rhombohedral shapes. Among these derivatives, 2H MoS_2 is a stable state, while 1T MoS_2 and 3R MoS_2 are metastable in nature.[25] The MoS_2 material has received special attention in the field of hydrogen evolution,[26,27] solar cells,[28] supercapacitors,[29] chemical sensors,[30] and gas sensors.[31] Recently, several methods were adapted to synthesize the MoS_2 material, such as chemical exfoliation method,[32] top-down and bottom-up processes like the soft template method,[33] chemical vapor deposition method,[34] electrospinning,[35] liquid phase sonication exfoliation,[36] hydrothermal/solvothermal method, and microwave synthesis.[37] Among these methods, the hydrothermally synthesized MoS_2 material has several advantages like eco-friendliness, less expensive, non-toxicity, good dispersion of the solution, and it can easily control the various morphology structures.[38]

In general, a supercapacitor electrode material highly depends on the surface morphology structure, electrical conductivity, and cyclic stability. Frangping Wang *et al.*[39] reported a flower-like MoS_2 microsphere morphology, which gives the maximum C_{sp} of 518.7 F g^{-1} at a current density of 1 A g^{-1}, and the cyclic stability retention is 88.2% after 2500 long cycles. Nikhitha Joseph *et al.*[40] reported a high electrical conductivity for the 1-T MoS_2 nanostructure with rich active edges, and achieved a maximum C_{sp} of 379 F g^{-1} at 1 A g^{-1}. Xiuhuawang *et al.*[41] demonstrated a 3-D structured MoS_2 nanoflower for the electrochemical properties, and observed a C_{sp} of 168 F g^{-1} at a current density of 1 A g^{-1}. The novelty of the present work is the synthesized MoS_2 nanoflower morphology with layered edges and nanosheet, in which the nanoflower MoS_2 shows the highest C_{sp} of 436.25 F g^{-1} at 10 mV s^{-1}. Furthermore, the GCD curve exhibits a maximum C_{sp} of 516 F g^{-1} at a current density of 1 A g^{-1}. It is a high C_{sp} compared to the previously reported MoS_2 material.[41]

In this present work, we reported the MoS_2 nanosheets and nanoflower synthesized by using the hydrothermal route in the presence of a soft template CTAB, which controls the surface morphology, shape, and size of the morphology structure. The CV curve shows the electrochemical double layer nature with a large loop. The GCD analysis reveals that the MoS_2 nanosheets and MoS_2 nanoflower electrode material is effective in supercapacitor device performance. The obtained results suggest that the MoS_2 nanoflower electrode material is a prominent candidate for energy storage and other applications.

2. Experimental methods

2.1 Materials used

Cetyltrimethylammonium bromide (CTAB), ammonium molybdate tetrahydrate (AMTH) thiourea, polyvinyl alcohol (PVA), potassium hydroxide (KOH), activated charcoal, and *N*-methyl-2 pyrrolidone (NMP) were obtained from Merck India, and polyvinylidene difluoride (PVDF) was purchased from Sigma Aldrich. Throughout the experiment, double-distilled water was used.

2.2 Synthesis of MoS_2 nanosheets and nanoflower morphology

The 2D-layered MoS_2 nanosheets were prepared by one-pot hydrothermal route. In this process, the precursor material ammonium molybdate tetrahydrate (AMTH) 16.184 (mmol) and 328.435 (mmol) thiourea were added to 80 ml of deionized water. Then, the mixed solution was sonicated about 30 minutes, and magnetically stirred for 30 minutes. The solution was further transferred to 100 ml of a Teflon-containing autoclave kit treated at 200 °C for about 48 hours. The collected MoS_2 black mixture product was centrifugated at 8000 rpm for about 30 minutes, and it was washed with water and ethanol, then vacuum dried at 50 °C for 8 hours.

Similarly, the MoS_2 nanoflower was synthesized by following the same procedure. In addition, 6 mmol of cation CTAB was added, which acted as a surfactant. It changed the nanosheet into nanoflower morphology due to the effect of the surface modifier. It is clearly represented in Scheme 1.

2.3 Characterization techniques

Characterization of the synthesized MoS_2 nanosheets and MoS_2 nanoflower active material morphology was carried out by using FESEM (Sigma-Zeiss), and HR-TEM measured through Titan (Themis 300 kV FEI), and the crystalline structure was examined by X-ray diffraction (XRD) techniques. The atomic percentage of the sample was analyzed through energy-dispersive X-ray spectroscopy (EDAX) and X-ray photoelectron spectroscopy (XPS) analyzed by Kartos axis ultra DLD (the used excitation source was monochromatic Al Kα and the emission angle was 90°; the spot size was 300 μm × 700 μm with 10^{-9} torr, Ultra-high vacuum). The chemical functional group of the material was characterized by ATR-FT-IR (alpha Bruker). The Brunauer Emmett Teller (BET) and Barrett Joyner Halenda (BJH) measurements were done by using a Quanta Chrome Instrument with a nitrogen adsorption/desorption environment.

2.4 Electrochemical characterization

Electrochemical techniques evaluated from cyclic voltammetry (CV), electrochemical Nyquist plot (EIS) and galvanostatic charging–discharging performance were carried out by using a computerized interface CHI 660E workstation.

3. Results and discussion

3.1 XRD pattern and FT-IR spectra analysis

Fig. 1(a) the XRD pattern was used to analyze the crystal structure of the synthesized MoS_2 nanosheets, and nanoflower diffraction peaks were observed at 14.28°, 33.56°, 40.0° and 59.01° and 14.04°, 33.34°, 39.53°, and 59.01°, and correspondingly indexed with the crystal planes (002), (101), (103), and (110), respectively.[42]

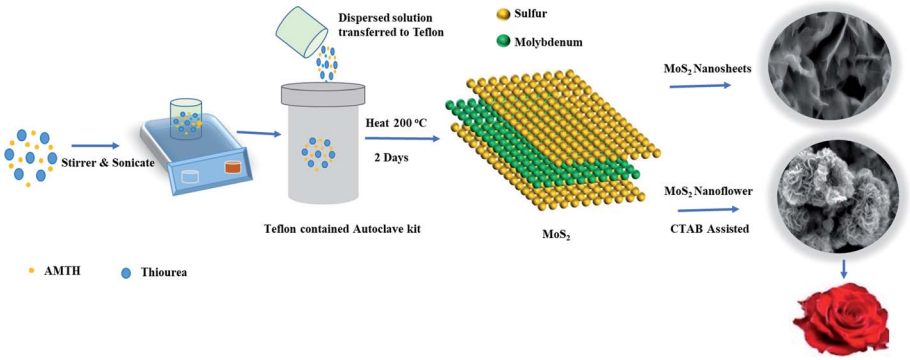

Scheme 1 Schematic illustration of the MoS_2 nanosheets and nanoflower morphology.

These characteristic peaks represent the presence of the hexagonal structure of MoS_2, and the highly intense peak observed at (002) reveals the good formation of a layered structure in the material. This crystal plane structure was well-defined with the previously reported results.[43] Fig. 1(b) shows the FT-IR spectra of the MoS_2 nanosheets, and MoS_2 nanoflower were carried out in the range of 4000 to 500 cm^{-1} to identify the chemical interaction, and functional groups are present in the electroactive material. The characteristic peaks observed at 601 cm^{-1} and 930 cm^{-1} are related to the Mo–S and S–S elements. The peaks shown at 1412 and 1617 cm^{-1} were assigned to the Mo–O functional group.[11] The broad peak observed at 1114 cm^{-1} is due to the aromatic ring C–H stretching and bending mode. The peak appeared at 715 cm^{-1} is due to bending out of the plane. The MoS_2 nanosheet peaks slightly shift towards lower intensity. These observed results clearly confirmed the proper chemical interaction and presence of the chemical functional groups and the change in the structural phase.

3.2 Surface morphology and elemental analysis of MoS_2 nanosheets and MoS_2 nanoflower

The surface morphology of the CTAB-assisted MoS_2 nanoflower and MoS_2 nanosheets (without CTAB) is shown in Fig. 2. It can be observed from the surface morphology of the MoS_2 nanosheets that surface is roughly covered by thin branched-like multi-layers and a sharp edge, as shown in Fig. 2(a). Fig. 2(b) displays the presence of CTAB in MoS_2 and shows that the flower (rose flower)-like structure with plenty of edges and nanoflower are arranged by the layers of petals, which enlarges the electroactive surface area mainly due to the presence of the CTAB surfactant. Obviously, defects appeared on the surface of MoS_2. They are responsible for the production of a greater number of active sites. Therefore, the active sites allow for assembling the holes and electron. They easily transport *via* the electrolytes during the device performance, which could allow for the large surface area. Furthermore, the created defects should help in easily transferring electrons as a result of the high electrical conductivity. It can be interpreted that the nanoflower is uniformly dispersed on the surface of MoS_2, and the surfactant CTAB is impacted on the morphology structure.

However, MoO_x and the thiourea mixture underwent a chemical reaction, and then nucleated in the synthesis process. Thiourea then releases the sulfur source under elevated temperature, and Mo is converted into a 2-D layered MoS_2 material. The formation of the MoS_2 chemical reaction is mentioned below.

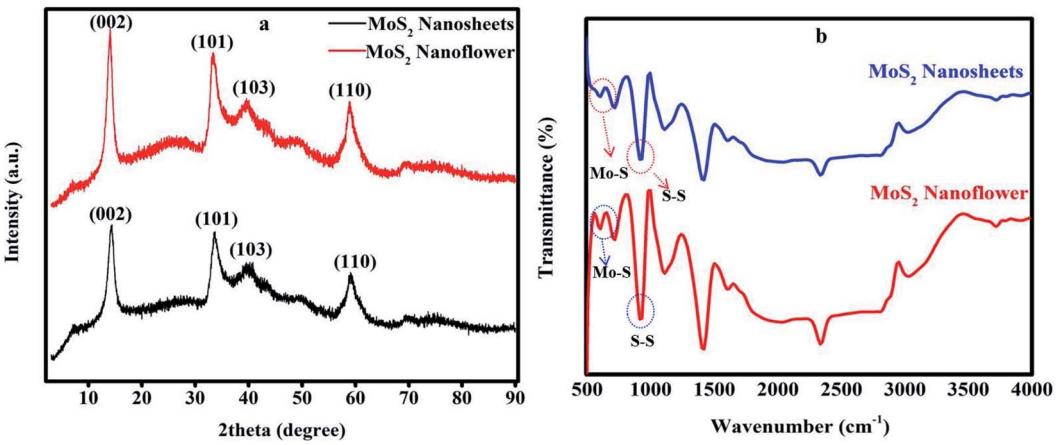

Fig. 1 (a) XRD pattern of the MoS_2 nanosheets and MoS_2 nanoflower. (b) FT-IR spectra of the MoS_2 nanosheets and MoS_2 nanoflower.

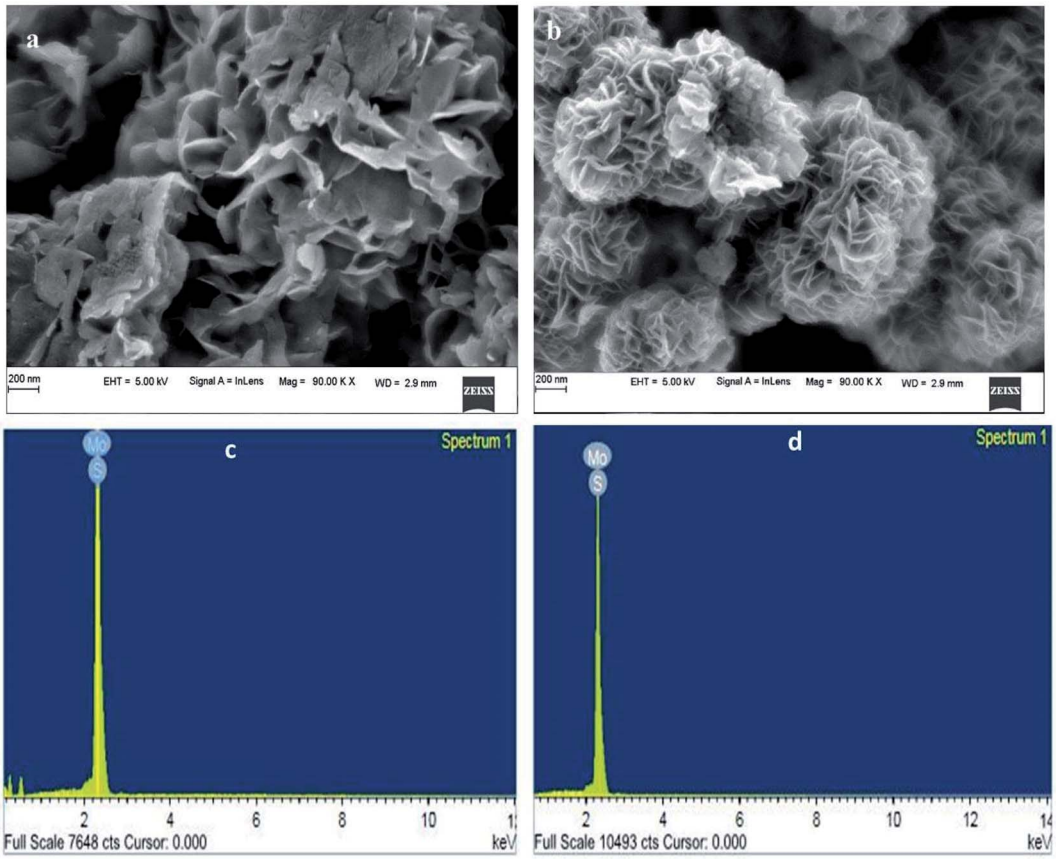

Fig. 2 (a and b) FESEM images of the MoS_2 nanosheets and MoS_2 nanoflower. (c and d) EDAX spectrum of the MoS_2 nanosheets and MoS_2 nanoflower.

$$CH_4N_2S + 2H_2O = 2NH_3 + CO_2 + H_2S^{2-}$$

$$(NH_4)_6Mo_7O_{24}\ \text{or}\ H_{32}Mo_7O_{24} = 6NH_3 + 7MoO_3 + 3H_2O$$

$$MoO_2 + 2H_2S = MoS_2 + 2H_2O$$

Fig. 2(c and d) shows the EDAX spectrum of the elemental study of the synthesized MoS_2 nanosheets, and the MoS_2 nanoflower clearly shows the presence of molybdenum (Mo) and sulphur (S) elements. The atomic percentages of S and Mo present in the nanosheet and nanoflower were indexed to 64.68% and 35.32%, and 65.49% and 34.51%, respectively. These results reveal that sulphur is more dominant than molybdenum.

3.3 HR-TEM image analysis of MoS_2 nanosheets and MoS_2 nanoflower

Fig. 3(a) shows the HR-TEM images of the MoS_2 nanosheets. It can be seen that the noticeable contrast between the sheet and few layers covered with each other. In Fig. 3(b), the MoS_2 nanoflower reveals the tightly packed multi-layers and thin nanosheet layers connected branch-like rose flower structure. Because of this, the natural rose flower demonstrated in Scheme 1 for comparison. In Fig. 3(c and d), the high resolutions HR-TEM images show the few layered structures and hexagonal shape defects presented on the surface of the MoS_2 layers. The d-spacing is 0.64 nm and ascribed to the (002) plane.[40] Fig. 3(e and f) SAED pattern of the MoS_2 nanosheets and MoS_2 nanoflower confirmed the hexagonal structure formation on MoS_2 and the *d*-spacing of 0.64 nm is consistent with the XRD indexed plane (002).

Obviously, the defects were generated at the edge sites and instantly influenced the reduction of the charge transfer resistance in the electroactive material, which may be helpful to improve the charge storage capacity. It was confirmed that the CTAB-assisted MoS_2 nanoflower morphology was more significant due to the CTAB surfactant effect, which established that the high active edges improves the surface area as a result.

3.4 X-ray photon spectroscopy of the MoS_2 nanoflower

The XPS spectra give the chemical nature and electronic structure of the composition, and the oxidation valence state of the MoS_2 nanoflower. Fig. 4(a) reveals the two broad Mo 3d distinguished peaks observed at 228.7 eV and 231.9 eV, which have been indexed to Mo^{4+} $3d_{5/2}$ and Mo^{4+} $3d_{3/2}$, respectively.

The deconvoluted peaks show the existence of 1T MoS_2 at 228.82 eV and 231.94 eV, while 2H-MoS_2 indicates the presence of two small peaks with corresponding binding energies at 229.8 eV and 233 eV. The 1T and 2H-phase peaks are consistent

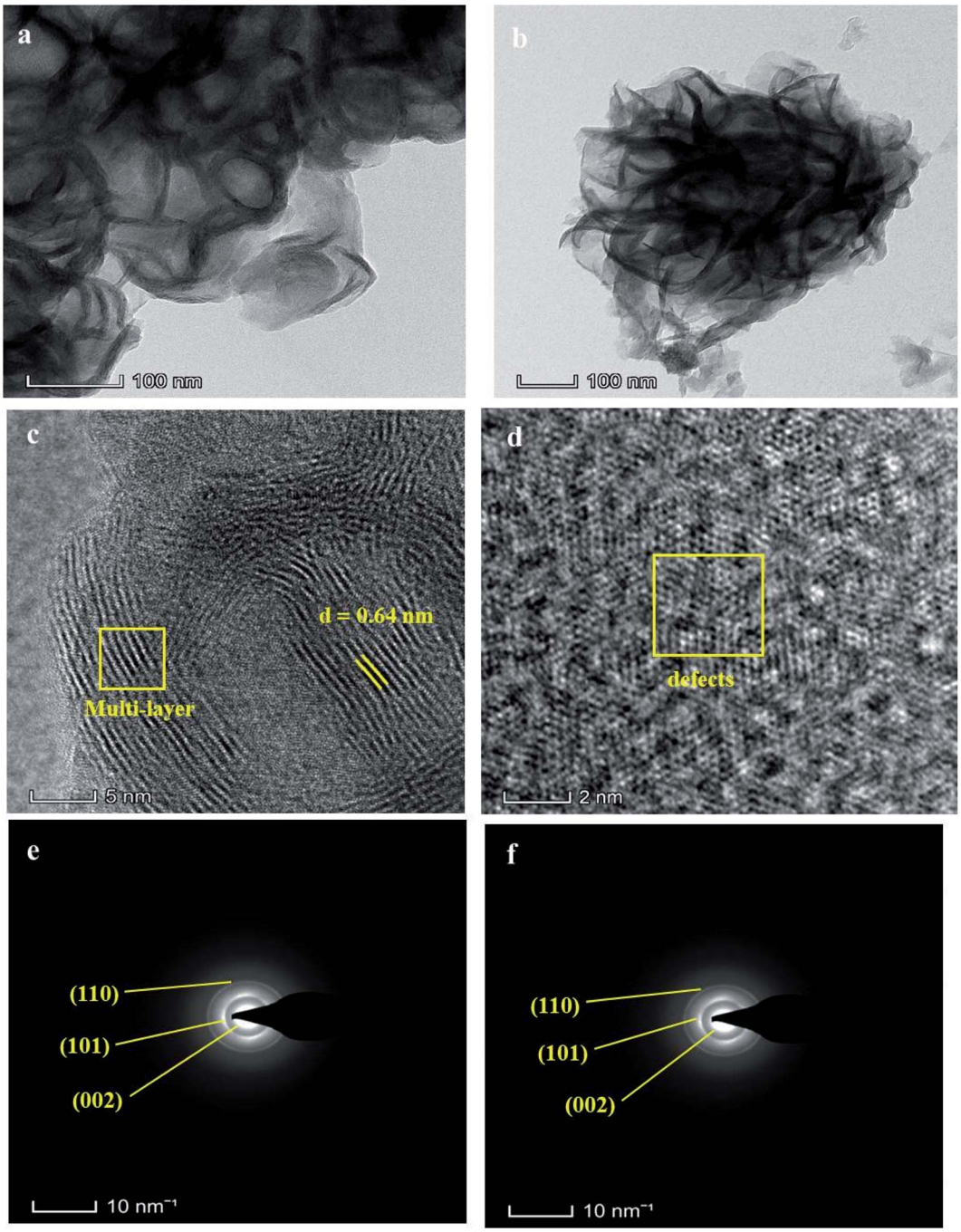

Fig. 3 HR-TEM images of the (a) MoS_2 nanosheets, (b) MoS_2 nanoflower, and (c and d) HR-TEM high resolutions images, (e and f) SAED pattern of MoS_2 nanosheets and MoS_2 nanoflower.

with the Mo 3d spectrum. The 1T-phase enhances the electrical conductivity due to the enhanced charge density or surface area, and the 2H-phase gives the stable state in nature. Here, it is observed that the two peaks at 234.8 eV and 236.06 eV are related to Mo^{6+} $3d_{5/2}$ and Mo^{6+} $3d_{3/2}$, respectively, and the S 2s attributed the binding energy at 225.90 eV.[44] Fig. 4(b) shows the S 2p spectrum. Strong peaks positioned at binding energies of 161.5 eV and 162.6 eV belong to S $2p_{3/2}$ and S $2p_{1/2}$, respectively.[45–47] All of these results confirm the oxidation state of the MoS_2 material.

3.5 BET surface area analysis of the MoS_2 nanosheets and MoS_2 nanoflower

The BET method was performed to investigate the specific surface area, pore size and volume distribution of the porous electroactive material in the nitrogen (N_2) adsorption/desorption environment.

Fig. 5(a) shows that the N_2 adsorption/desorption isotherms of the MoS_2 nanosheets and MoS_2 nanoflower exhibit type IV characteristics with a hysteresis loop, which suggests the

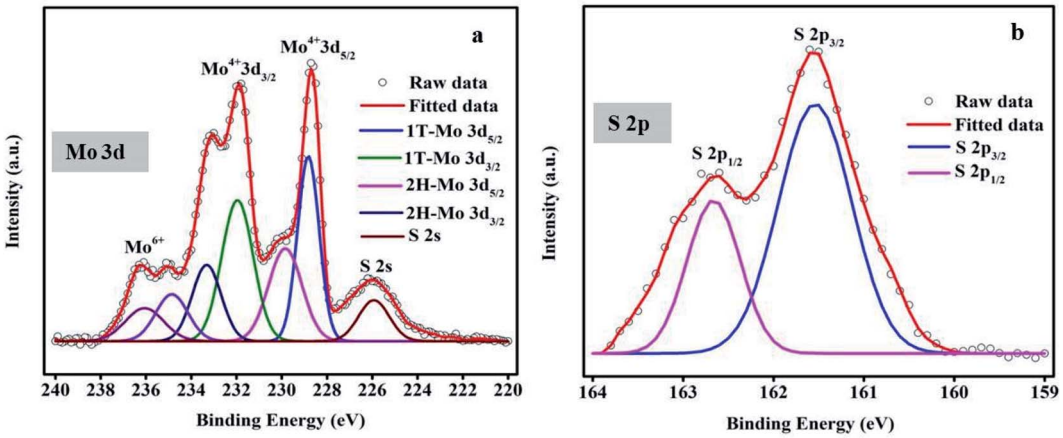

Fig. 4 XPS spectra of the MoS_2 nanoflower: (a) Mo 3d, (b) S 2p.

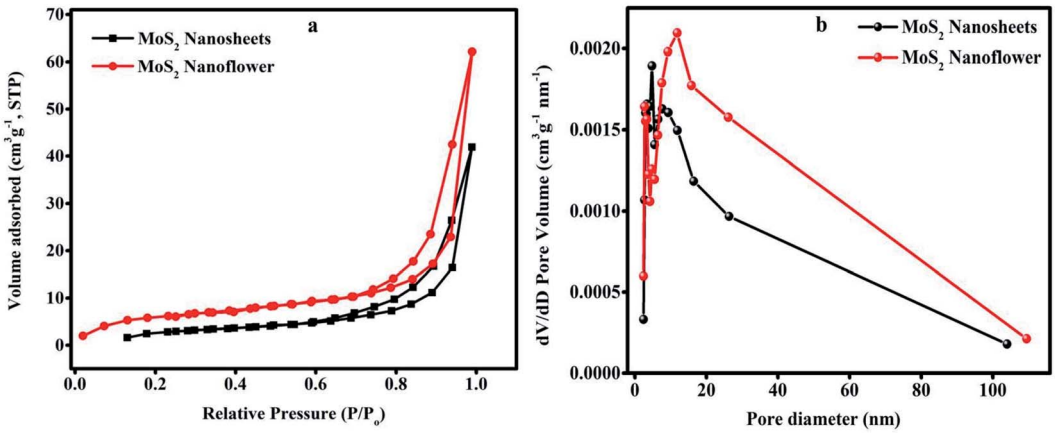

Fig. 5 (a) N_2 adsorption and desorption isotherms. (b) BJH Pore size distribution curves of the MoS_2 nanosheets and MoS_2 nanoflower.

presence of a mesoporous structure and large pores. The specific surface area of the MoS_2 nanoflower (20.419 m^2 g^{-1}) is much higher than that of the MoS_2 nanosheets (16.334 m^2 g^{-1}). Fig. 5(b) shows the BJH pore diameter size and volume distribution curves. The observed pore size is about 4.829 nm and 11.852 nm for the MoS_2 nanosheets and MoS_2 nanoflower, respectively. The large specific surface area obtained in the MoS_2 nanoflower is mainly due to the petals of the layered edges and more mesoporous pores. This can offer a greater number of active sites and enhances the surface area, which is beneficial for the supercapacitor application.

4. Supercapacitor property of the MoS_2 nanosheets and MoS_2 nanoflower

To fabricate the working electrode on copper foil, the first copper foil was cleaned with acetone and dried at ambient temperature. The material composition is chosen in weight ratios of MoS_2 active material/activated charcoal/PVDF (80 : 15 : 5), which were mixed with a NMP solution to form a slurry. It was coated on the copper foil electrode surface using a doctor blade method, then dried in a vacuum oven at 60 °C about 12 hours. The prepared electrode is used as a working electrode in a two-electrode configuration. The CV curve performance was done in the range between −0.8 to 0.6 V applied potential window with various scan rates. The galvanostatic charging–discharging (GCD) curve is measured at different current densities. The electrochemical behaviour of the MoS_2 nanosheet and MoS_2 nanoflower electrode materials was investigated by using a two-electrode system.

The Fig. 6(a) CV plots show the symmetric shape of the oxidation and redox reaction curve at a scan rate of 30 mV s^{-1}. The MoS_2 nanoflower electrode shows a large surface area CV curve and higher current rate than the MoS_2 nanosheets because it undergoes a more faradaic site reaction. The Fig. 6(b and c) CV profile was recorded at different scan rates from 10 mV s^{-1} to 50 mV s^{-1}. The observed CV curves simultaneously shift towards the positive and negative current rate. It is clearly observed from the CV curve that it maintains a similar shape with a wide area, signifying the strong electrochemical double-layer capacitor properties. It can be interpreted that the MoS_2 nanoflower morphology

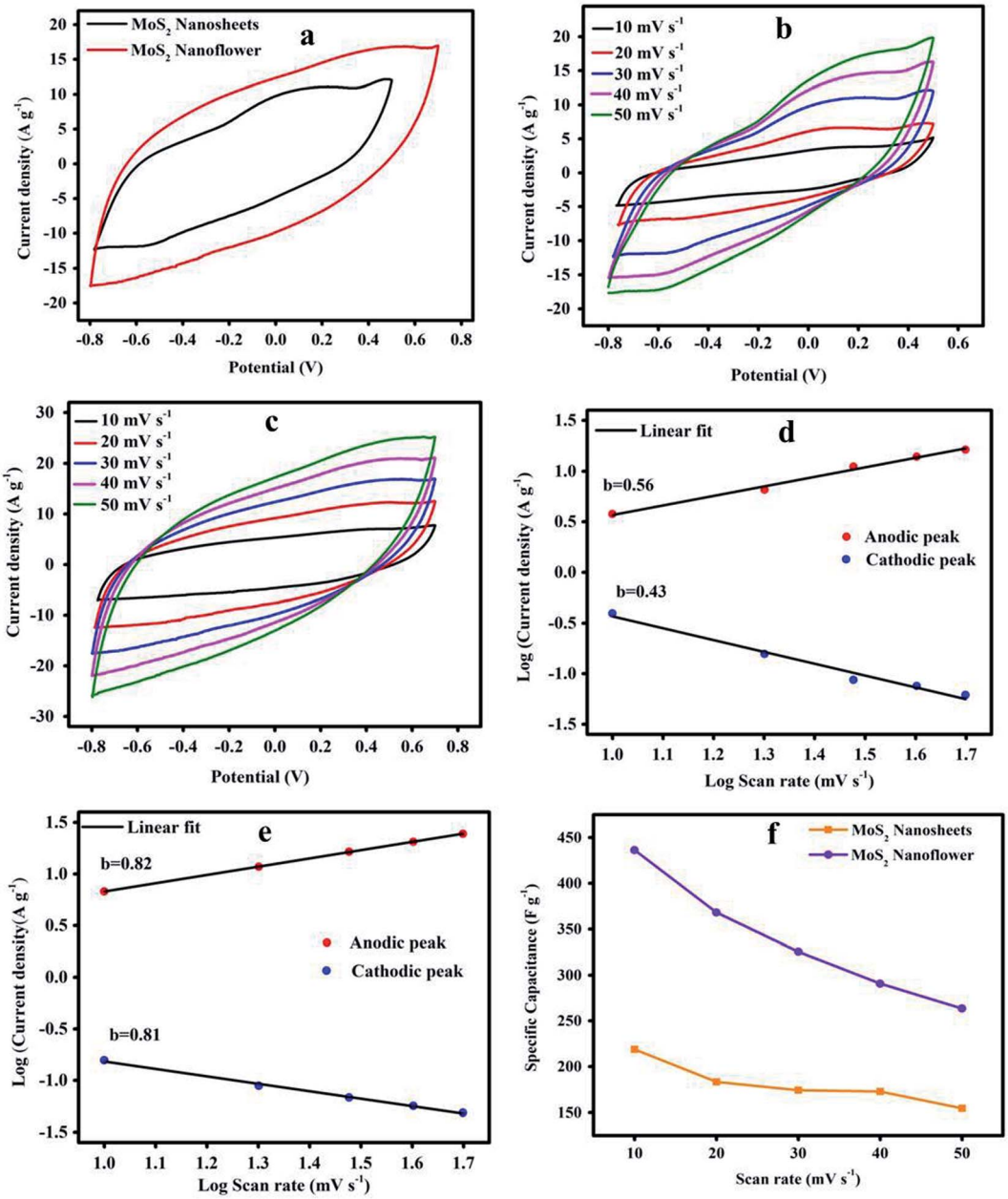

Fig. 6 CV images of the (a) MoS_2 nanosheets and MoS_2 nanoflower at a scan rate of 30 mV s^{-1}. (b and c) MoS_2 nanosheets and MoS_2 nanoflower at various scan rates. (d and e) The log scan rate against the log current density, and (f) the scan rate proportional to the capacitance.

electrode active material is more stable. The PVA/KOH gel electrolyte ion reacts with the MoS_2 electrode active material, and quickly creates a fast electron transfer due to the low resistance of the active material and kinetic reaction dynamics. Obviously, the MoS_2 material at a low scan rate provides a faradaic behaviour capacitance, which plays a crucial role in increasing the charge storage capacitive nature.[48] The MoS_2 nanoflower has a higher current density than the MoS_2 nanosheets with an applied potential from −0.8 to 0.6 V.

Figure 6(d and e) shows the log current density (I_P) *versus* log scan rate (anodic and cathodic peak), which is the linear affinity between the log V (scan rate). As per the Power-law ($I_P = av^b$) the "b" value is determined from the slope of log(V) *versus* log(I_P) "a" and is a constant. The parameter of the "b" value is 0.5 and represents the controlled diffusion properties, and 1 is the capacitive behaviour.[49] The obtained slopes for the MoS_2 nanosheets and MoS_2 nanoflower of the anodic and cathodic peaks expressed the "b" values of 0.43, 0.56, and 0.81, 0.82, respectively. It can be emphasized that the MoS_2 nanosheets indicate the controlled diffusion process, and the MoS_2 nanoflower non-controlled diffusion process or capacitive behaviour due to the cause of polarization, and the high current response, as well as rapid reversible redox reaction.[50]

Fig. 6(f) shows the capacitance of the MoS_2 nanosheets and MoS_2 nanoflower electrode material. The wide area of the CV curve was calculated by using the following relation:

$$C_{sp} = \frac{1}{(V_2 - V_1)\nu \times 2m} \int_{\nu_1}^{\nu_2} I(V)\mathrm{d}V$$

where $I(V)\mathrm{d}V$ is the integral area of the CV plot, $(V_2 - V_1)$ is the applied potential range, ν is the scan rate, and m is the mass of the electroactive material. It was observed that the C_{sp} was 218.88 F g^{-1} and 436.26 F g^{-1} for the MoS_2 nanosheets and nanoflower electrode material, respectively, at a slow scan rate of 10 mV s^{-1}. The MoS_2 nanoflower exhibits excellent capacitive storage capacity due to the high surface area.

GCD analysis of the MoS_2 nanosheets and MoS_2 nanoflower

In Fig. 7(a and b), the GCD curve of the MoS_2 nanosheets and nanoflower electrode material shows a capacitive nature and slightly deviated from the triangular shape. The MoS_2 electrode material is highly active for the PVA/KOH gel electrolyte due to the high intrinsic ion fast diffusion process, and the obtained results clearly showed the outstanding synergetic effect of the electrode capacity performance.

The C_{sp} of the electroactive material was determined from the GCD curve at various current densities using the following expression:[51]

$$C_{sp} = (I\Delta t)/m\Delta V$$

where I is the applied current, Δt is the discharging time, m is the mass of the electrode active material, and ΔV is the total potential variation of the discharging curve.

Fig. 7(c) shows the MoS_2 nanosheets and nanoflower electrode C_{sp} *versus* the current density. We can observe that at the current density of 1 A g^{-1} to 2.5 A g^{-1}, the C_{sp} correspondingly found decreases from 438 F g^{-1} to 159.23 F g^{-1}, and 516 F g^{-1} to 200.69 F g^{-1}, which are clearly displayed from the downward tendency specific capacitance curve. The MoS_2 nanoflower exhibits a high C_{sp} of 516 F g^{-1} at 1 A g^{-1} current density compared with the MoS_2 nanosheets.

The observed C_{sp} value of the nanoflower clearly signifies the improvement in the energy storage capacity due to the presence of defects, plenty of edge sites, stable state of the electrode material, high intrinsic ion conductivity, and interface relation between the electrode material surface and electrolyte. The obtained data agreed well with the previously reported values, as mentioned in Table 1.

Fig. 7(d) is the graph of the electrochemical impedance spectroscopy (EIS) results measured to investigate the interface resistance contact between the electrode active material and electrolyte. According to the Nyquist plot, the quasi-semicircle with the charge transfer resistance (R_{ct}) value shows the MoS_2 nanosheets is 4.86 Ohm and the MoS_2 nanoflower is 3.40 Ohm.

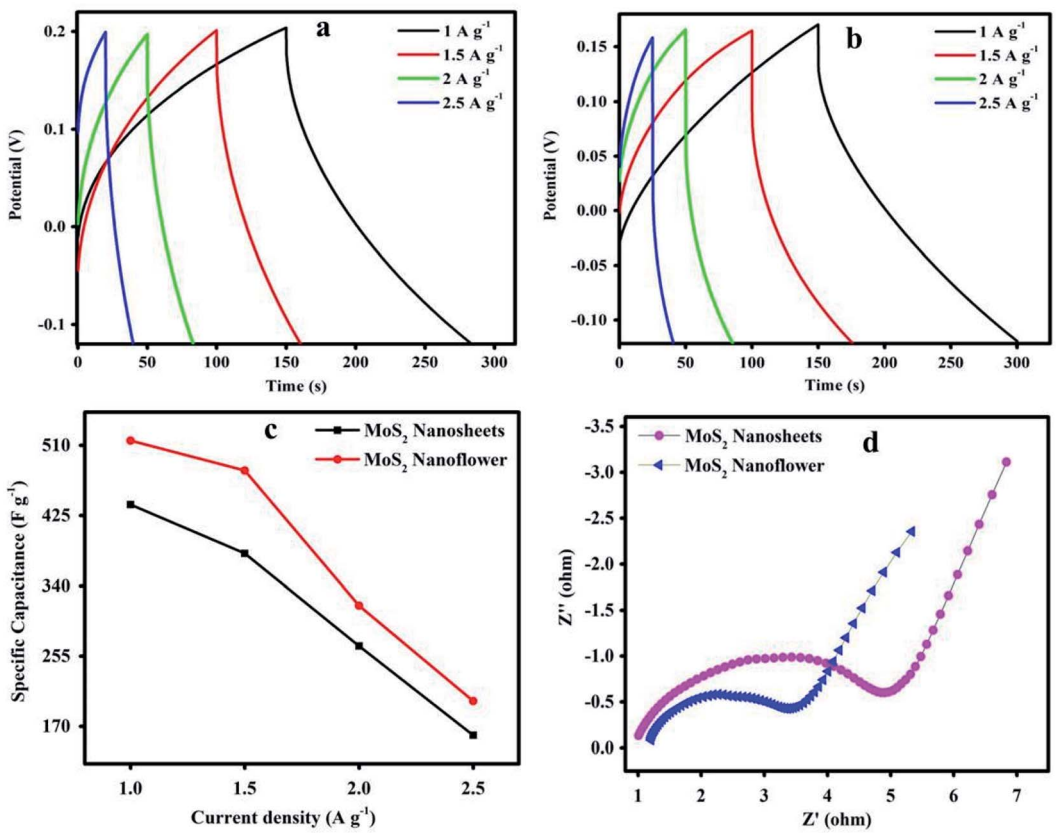

Fig. 7 GCD curve of the (a) MoS_2 nanosheets, (b) MoS_2 nanoflower. (c) MoS_2 nanosheets and MoS_2 nanoflower current density *versus* C_{sp}, and (d) Nyquist plot of the MoS_2 nanosheets and MoS_2 nanoflower.

Table 1 The specific capacitance (C_{sp}) of different MoS_2 electrode materials at the current density of 1 A g^{-1}

Electrode material	Electrolytes	C_{sp} F g^{-1}	References
Metallic 1T-MoS_2	1 M KOH	379	40
MoS_2/graphene	1 M Na_2So_4	243	48
Flower-like MoS_2 nanostructure	1 M KCl	168	41
MoS_2/PPy	1 M H_2So_4	400	56
MoS_2/PANI	0.5 M H_2So_4	450	57
BCN/MoS_2	1 M H_2So_4	283	58
MoS_2 nanosheets	PVA/KOH	438	This work
MoS_2 nanoflower	PVA/KOH	516	This work

The MoS_2 nanoflower material possesses a small R_{ct} value. It may offer high electrical conductivity, and also reveals the faster electron transfer and ion diffusion process. Overall, the MoS_2 electrode contributed high electrochemical performance in accordance with the supercapacitor device application. CTAB is a cationic surfactant used in the synthesis, and it is responsible for changing the surface morphology of the MoS_2 nanosheets into a MoS_2 nanoflower. The CTAB-assisted MoS_2 nanoflower established more edge layer structure and atomic defects on the surface. It can also be interpreted that the layered edges easily possess the quick transfer of electrons in the electrochemical mechanism.

The cyclic stability of the MoS_2 nanosheets and MoS_2 nanoflower electrode was performed by GCD technique at a current density of 2.5 A g^{-1} for 2000 cycles, as shown in Fig. 8 (inset). The MoS_2 nanosheets and MoS_2 nanoflower electrode possess 83.3% and 87.42% capacitance retention after 2000 cycles. The MoS_2 nanoflower exhibits higher capacitance retention than those previously reported MoS_2-based results. For example, the MoS_2/rGO/PPy/ITO[52] supercapacitor electrode shows 76.68% of the capacitance retention, the MoS_2/PANI[53] core shell composite electrode exhibits 86% capacitance retention after 1000 cycles, the MoS_2 sponge electrode shows 80% capacitance retention,[54] and the MoS_2/PANI-38 (ref. 55) composite electrode shows 86% capacitance retention. The observed results clearly reveal that the MoS_2 nanoflower electrode materials are highly favorable for supercapacitor application.

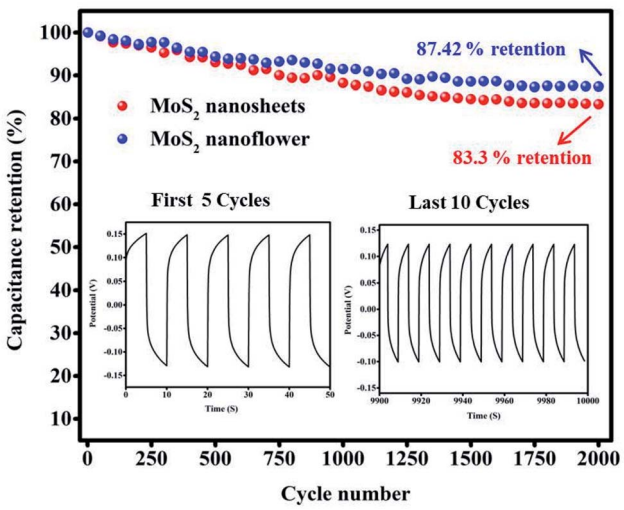

Fig. 8 The cyclic stability analysis of the MoS_2 nanosheets and the MoS_2 nanoflower (inset figure: first 5 cycles and last 10 cycles).

Conclusions

The MoS_2 nanosheets and CTAB-assisted nanoflower were successfully synthesized by using the hydrothermal route, and the MoS_2 material confirmed the presence of the chemical constituents S–S and Mo–S by FT-IR spectra. The XRD indexed plane (002) intense peak reveals the hexagonal structure formation of the MoS_2 material. The FESEM and HR-TEM images confirm the presence of nanosheets and the nanoflower morphology. The EDAX spectrum of the elemental study suggested that sulphur is more dominant than molybdenum, and the XPS graph demonstrates the presence of Mo and S elements. The MoS_2 nanoflower CV curve exhibits the electrical double layer capacitance nature with a large loop. The maximum capacitance achieved by 436.26 F g^{-1} at 10 mV s^{-1} and C_{sp} from GCD found at 516 F g^{-1} at the current density of 1 A g^{-1}, and the MoS_2 nanosheets electrode shows the C_{sp} from CV and GCD of 218.88 F g^{-1} at 10 mV s^{-1} and 438 F g^{-1} at the current density of 1 A g^{-1}. These results confirmed that the MoS_2 nanoflower had a greater capacitance magnitude than the MoS_2 nanosheets electrode active material due to the nanoflower having a large surface area, and these materials are suitable for the high potential energy storage applications of the supercapacitor.

Conflicts of interest

There is no conflicts of interest.

Acknowledgements

The authors acknowledge Mangalore University for providing a research fellowship, the PURSE LAB, Mangalore University, and the IISc, Department of Centre for Nanoscience, Bangalore for the characterization facility.

References

1 L. Ren, G. Zhang, Z. Yan, L. Kang, H. Xu, F. Shi and Z. H. Liu, Three-dimensional tubular MoS_2/PANI hybrid electrode for high rate performance supercapacitor, *ACS Appl. Mater. Interfaces*, 2015, **7**, 28294–28302.
2 M. Mohan, K. N. Unni and R. B. Rakhi, 2D organic-inorganic hybrid composite material as a high-performance supercapacitor electrode, *Vacuum*, 2019, **166**, 335–340.
3 M. Li, J. Lu, K. Luo, Y. Li, K. Chang, K. Chen and Q. Huang, Element replacement approach by reaction with Lewis acidic molten salts to synthesize nano laminated MAX phases and MXenes, *J. Am. Chem. Soc.*, 2019, **141**, 4730–4737.
4 J. He, G. Hartmann, M. Lee, G. S. Hwang, Y. Chen and A. Manthiram, Freestanding 1T MoS_2/graphene

heterostructures as a highly efficient electrocatalyst for lithium polysulfides in Li–S batteries, *Energy Environ. Sci.*, 2019, **12**, 344–350.

5 T. T. Shan, S. Xin, Y. You, H. P. Cong, S. H. Yu and A. Manthiram, Combining nitrogen-doped graphene sheets and MoS2: a unique film–foam–film structure for enhanced lithium storage, *Angew. Chem. Int. Ed.*, 2016, **55**, 12783–12788.

6 Q. Tao, M. Dahlqvist, J. Lu, S. Kota, R. Meshkian, J. Halim and J. Rosen, Two-dimensional Mo 1.33 C MXene with divacancy ordering prepared from parent 3D laminate with in-plane chemical ordering, *Nat. Commun.*, 2017, **8**, 1–7.

7 F. Lan, H. Zhang, J. Fan, Q. Xu, H. Li and Y. Min, Electrospun Polymer Nanofibers with TiO_2@ NiCo-LDH as Efficient Polysulfide Barriers for Wide-Temperature-Range Li–S Batteries, *ACS Appl. Mater. Interfaces*, 2021, **13**, 2734–2744.

8 H. He, Y. Chai, X. Zhang, P. Shi, J. Fan, Q. Xu and Y. Min, A 2D–3D co-conduction effect in PEO-based all-solid-state batteries for long term cycle stability, *J. Mater. Chem. A*, 2021, **9**, 9214–9227.

9 L. Ren, G. Zhang, Z. Yan, L. Kang, H. Xu, F. Shi and Z. H. Liu, Three-dimensional tubular MoS_2/PANI hybrid electrode for high rate performance supercapacitor, *ACS Appl. Mater. Interfaces*, 2015, **7**, 28294–28302.

10 A. Ratan, A. Tripathi and V. Singh, Swift heavy ion beam modified MoS_2-PVA nanocomposite free-standing electrodes for polymeric electrolyte based asymmetric supercapacitor, *Vacuum*, 2021, **184**, 109992.

11 K. J. Huang, J. Z. Zhang, G. W. Shi and Y. M. Liu, Hydrothermal synthesis of molybdenum disulfide nanosheets as supercapacitors electrode material, *Electrochim. Acta*, 2014, **132**, 397–403.

12 W. J. Zhang and K. J. Huang, A review of recent progress in molybdenum disulfide-based supercapacitors and batteries, *Inorg. Chem. Front.*, 2017, **4**, 1602–1620.

13 K. V. G. Raghavendra, C. V. M. Gopi, R. Vinodh, I. K. Durga and H. J Kim, One-step facile synthesis of dense cloud-like tiny bundled nanoparticles of CuS nanostructures as an efficient electrode material for high-performance supercapacitors, *J. Energy Storage*, 2020, **27**, 101148.

14 G. S. Selopal, R. Chahine, M. Mohammadnezhad, F. Navarro-Pardo, D. Benetti, H. Zhao and F. Rosei, Highly efficient and stable spray assisted nanostructured $Cu2_S$/Carbon paper counter electrode for quantum dots sensitized solar cells, *J. Power Sources*, 2019, **436**, 226849.

15 S. Ahmad, C. Yang, W. Xie, Z. Deng, H. Zhang, Y. Zhao and X. Su, Molten salt-templated synthesis of ternary NiS–$NiCo_2O_4$@ C composites as high performance catalysts for 4-nitro phenol reduction and supercapacitor, *Carbon*, 2020, **158**, 912–921.

16 Y. Liu, W. Li, X. Chang, H. Chen, X. Zheng, J. Bai and Z. Ren, $MoSe_2$ nanoflakes-decorated vertically aligned carbon nanotube film on nickel foam as a binder-free supercapacitor electrode with high rate capability, *J. Colloid Interface Sci.*, 2020, **562**, 483–492.

17 H. Chu, F. Zhang, L. Pei, Z. Cui, J. Shen and M. Ye, Ni, Co and Mn doped SnS_2-graphene aerogels for supercapacitors, *J. Alloys Compd.*, 2018, **767**, 583–591.

18 Y. You, K. Qu, C. Shi, Z. Sun, Z. Huang, J. Li and Z. Guo, Binder-free CuS/ZnS/sodium alginate/rGO nanocomposite hydrogel electrodes for enhanced performance supercapacitors, *Int. J. Biol. Macromol.*, 2020, **162**, 310–319.

19 M. Dakshana, S. Meyvel, M. Malarvizhi, P. Sathya, R. Ramesh, S. Prabhu and M. Silambarasan, Facile synthesis of $CuCo_2S_4$ nanoparticles as a faradaic electrode for high performance supercapacitor applications, *Vacuum*, 2020, **174**, 109218.

20 C. Zhao, X. Shao, Z. Zhu, C. Zhao and X. Qian, One-pot hydrothermal synthesis of RGO/FeS composite on Fe foil for high performance supercapacitors, *Electrochim. Acta*, 2017, **246**, 497–506.

21 P. Geng, S. Zheng, H. Tang, R. Zhu, L. Zhang, S. Cao and H. Pang, Transition metal sulfides based on graphene for electrochemical energy storage, *Adv. Energy Mater.*, 2018, **8**, 1703259.

22 S. Gong, J. Fan, V. Cecen, C. Huang, Y. Min, Q. Xu and H. Li, Noble-metal and cocatalyst free W_2N/C/TiO photocatalysts for efficient photocatalytic overall water splitting in visible and near-infrared light regions, *Chem. Eng. J.*, 2021, **405**, 126913.

23 C. Li, J. Li, Z. Wang, S. Zhang, G. Wei, J. Zhang and C. An, The synthesis of hollow MoS_2 nanospheres assembled by ultrathin nanosheets for an enhanced energy storage performance, *Inorg. Chem. Front.*, 2017, **4**, 309–314.

24 C. Zeng, J. Pu, H. Wang, S. Zheng and R. Chen, Influence of microstructure on tribological properties and corrosion resistance of MoS_2/WS_2 films, *Ceram. Int.*, 2020, **46**, 13774–13783.

25 G. Feng, A. Wei, Y. Zhao and J. Liu, Synthesis of flower-like MoS_2 nanosheets microspheres by hydrothermal method, *J. Mater. Sci.: Mater. Electron.*, 2015, **26**, 8160–8166.

26 D. Voiry, M. Salehi, R. Silva, T. Fujita, M. Chen, T. Asefa and M. Chhowalla, Conducting MoS_2 nanosheets as catalysts for hydrogen evolution reaction, *Nano Lett.*, 2013, **13**, 6222–6227.

27 L. Li, Z. Qin, L. Ries, S. Hong, T. Michel, J. Yang and D. Voiry, Role of sulfur vacancies and undercoordinated Mo regions in MoS_2 nanosheets toward the evolution of hydrogen, *ACS Nano*, 2019, **13**, 6824–6834.

28 E. Singh, K. S. Kim, G. Y. Yeom and H. S. Nalwa, Atomically thin-layered molybdenum disulfide (MoS_2) for bulk-heterojunction solar cells, *ACS Appl. Mater. Interfaces*, 2017, **9**, 3223–3245.

29 J. Chao, J. Deng, W. Zhou, J. Liu, R. Hu, L. Yang and O. G. Schmidt, Hierarchical nanoflowers assembled from MoS_2/polyaniline sandwiched nanosheets for high-performance supercapacitors, *Electrochim. Acta*, 2017, **243**, 98–104.

30 H. Y. Chen, J. Wang, L. Meng, T. Yang and K. Jiao, Thin-layered MoS_2/polyaniline nanocomposite for highly sensitive electrochemical detection of chloramphenicol, *Chin. Chem. Lett.*, 2016, **27**, 231–234.

31 Y. Han, D. Huang, Y. Ma, G. He, J. Hu, J. Zhang and Z. Yang, Design of hetero-nanostructures on MoS_2 nanosheets to

boost NO_2 room-temperature sensing, *ACS Appl. Mater. Interfaces*, 2018, **10**, 22640–22649.

32 L. Maachou, K. Qi, E. Petit, Z. Qin, Y. Zhang, D. Cot and D. Voiry, Biomimetic electro-oxidation of alkyl sulfides from exfoliated molybdenum disulfide nanosheets, *J. Mater. Chem. A*, 2020, **8**, 25053–25060.

33 Z. Wang and B. Mi, Environmental applications of 2D molybdenum disulfide (MoS_2) nanosheets, *Environ. Sci. Technol.*, 2017, **51**, 8229–8244.

34 A. Zobel, A. Boson, P. M. Wilson, D. S. Muratov, D. V. Kuznetsov and A. Sinitskii, Chemical vapour deposition and characterization of uniform bilayer and trilayer MoS_2 crystals, *J. Mater. Chem. C*, 2016, **4**, 11081–11087.

35 S. Liu, X. Zhang, H. Shao, J. Xu, F. Chen and Y. Feng, Preparation of MoS_2 nanofibers by electrospinning, *Mater. Lett.*, 2012, **73**, 223–225.

36 J. Yang, K. Wang, J. Zhu, C. Zhang and T. Liu, Self-templated growth of vertically aligned 2H-1T MoS_2 for efficient electrocatalytic hydrogen evolution, *ACS Appl. Mater. Interfaces*, 2016, **8**, 31702–31708.

37 A. Asok, A. A. Naik, S. Arunachalam, R. Govindaraj and K. Haribabu, Microwave assisted synthesis of polythiophene–molybdenum sulfide counter electrode in dye-sensitized solar cell, *J. Mater. Sci.: Mater. Electron.*, 2019, **30**, 13655–13663.

38 J. Zhao, Y. Zhang, Y. Wang, H. Li and Y. Peng, The application of nanostructured transition metal sulfides as anodes for lithium ion batteries, *J. Energy Chem.*, 2018, **27**, 1536–1554.

39 F. Wang, G. Li, J. Zheng, J. Ma, C. Yang and Q. Wang, Hydrothermal synthesis of flower-like molybdenum disulfide microspheres and their application in electrochemical supercapacitors, *RSC Adv.*, 2018, **8**, 38945–38954.

40 N. Joseph, P. M. Shafi and A. C. Bose, Metallic 1T-MoS_2 with defect induced additional active edges for high performance supercapacitor application, *New J. Chem.*, 2018, **42**, 12082–12090.

41 X. Wang, J. Ding, S. Yao, X. Wu, Q. Feng, Z. Wang and B. Geng, High supercapacitor and adsorption behaviors of flower-like MoS_2 nanostructures, *J. Mater. Chem. A*, 2014, **2**, 15958–15963.

42 R. Khatri and N. K. Puri, Electrochemical study of hydrothermally synthesised reduced MoS_2 layered nanosheets, *Vacuum*, 2020, **175**, 109250.

43 W. Li, Y. Shen, X. Xiao, C. An, G. Wei, Y. Wang and C. An, Simple Te-Thermal Converting 2H to 1T@ 2H MoS_2 Homojunctions with Enhanced Supercapacitor Performance, *ACS Appl. Energy Mater.*, 2019, **2**, 8337–8344.

44 X. Gao, M. Hu, J. Sun, Y. Fu, J. Yang, W. Liu and L. Weng, Response of RF-sputtered MoS_2 composite films to LEO space environment, *Vacuum*, 2017, **144**, 72–79.

45 N. Zhang, W. Ma, T. Wu, H. Wang, D. Han and L. Niu, Edge-rich MoS_2 nanosheets rooting into polyaniline nanofibers as effective catalyst for electrochemical hydrogen evolution, *Electrochim. Acta*, 2015, **180**, 155–163.

46 J. Chao, L. Yang, J. Liu, R. Hu and M. Zhu, Oxygen-incorporated and polyaniline-intercalated 1T/2H hybrid MoS_2 nanosheets arrayed on reduced graphene oxide for high-performance supercapacitors, *J. Phys. Chem. C*, 2018, **122**, 8128–8136.

47 C. Nethravathi, J. Prabhu, S. Lakshmipriya and M. Rajamathi, Magnetic Co-doped MoS_2 nanosheets for efficient catalysis of nitroarene reduction, *ACS Omega*, 2017, **2**, 5891–5897.

48 K. J. Huang, L. Wang, Y. J. Liu, Y. M. Liu, H. B. Wang, T. Gan and L. L. Wang, Layered MoS_2–graphene composites for supercapacitor applications with enhanced capacitive performance, *Int. J. Hydrogen Energy*, 2013, **38**, 14027–14034.

49 S. Liu, Y. Yin, K. S. Hui, K. N. Hui, S. C. Lee and S. C. Jun, High-performance flexible quasi-solid-state supercapacitors realized by molybdenum dioxide@ nitrogen-doped carbon and copper cobalt sulfide tubular nanostructures, *Adv. Sci.*, 2018, **5**, 1800733.

50 Y. Zhu, H. Huang, G. Li, X. Liang, W. Zhou, J. Guo and S. Tang, Graphene-anchored $NiCoO_2$ nanoarrays as supercapacitor electrode for enhanced electrochemical performance, *Electrochim. Acta*, 2017, **248**, 562–569.

51 H. Vijeth, S. P. Ashokkumar, L. Yesappa, M. Vandana and H. Devendrappa, Hybrid core-shell nanostructure made of chitosan incorporated polypyrrole nanotubes decorated with NiO for all-solid-state symmetric supercapacitor application, *Electrochim. Acta*, 2020, **354**, 136651.

52 D. Sarmah and A. Kumar, Layer-by-layer self-assembly of ternary MoS_2-rGO@PPyNTs nanocomposites for high performance supercapacitor electrode, *Synth. Met.*, 2018, **243**, 75–89.

53 X. Zhang, L. Ma, M. Gan, G. Fu, M. Jin and Y. Zhai, Controllable constructing of hollow MoS_2/PANI core/shell microsphere for energy storage, *Appl. Surf. Sci.*, 2018, **460**, 48–57.

54 S. K. Balasingam, M. Lee, B. H. Kim, J. S. Lee and Y. Jun, Freeze-dried MoS_2 sponge electrodes for enhanced electrochemical energy storage, *Dalton Trans.*, 2017, **46**, 2122–2128.

55 J. Wang, Z. Wu, K. Hu, X. Chen and H. Yin, High conductivity graphene-like MoS_2/polyaniline nanocomposites and its application in supercapacitor, *J. Alloys Compd.*, 2015, **619**, 38–43.

56 A. K. Thakur, R. B. Choudhary, M. Majumder, G. Gupta and M. V. Shelke, Enhanced electrochemical performance of polypyrrole coated MoS_2 nanocomposites as electrode material for supercapacitor application, *J. Electroanal. Chem.*, 2016, **782**, 278–287.

57 J. Lei, Z. Jiang, X. Lu, G. Nie and C. Wang, Synthesis of few-layer MoS_2 nanosheets-wrapped polyaniline hierarchical nanostructures for enhanced electrochemical capacitance performance, *Electrochim. Acta*, 2015, **176**, 149–155.

58 A. K. Thakur, M. Majumder, R. B. Choudhary and S. B. Singh, MoS_2 flakes integrated with boron and nitrogen-doped carbon: striking gravimetric and volumetric capacitive performance for supercapacitor applications, *J. Power Sources*, 2018, **402**, 163–173.